Supporting information

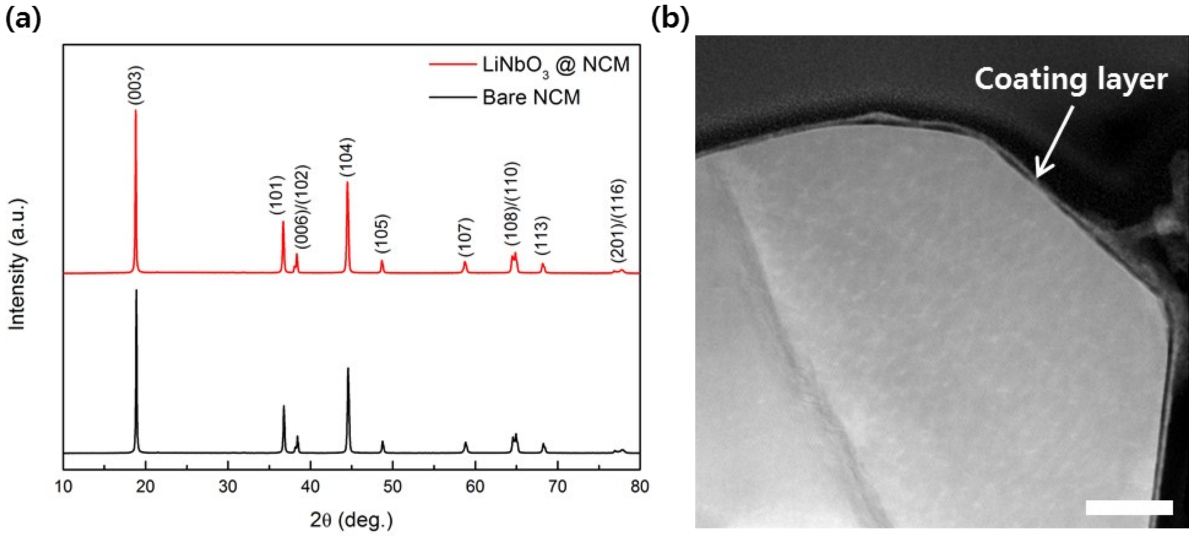

Figure S1. (a) XRD patterns of bare NCM powder and $LiNbO_3$-coated NCM powder. (b) TEM image of $LiNbO_3$-coated NCM. Scale bar is 50 nm.

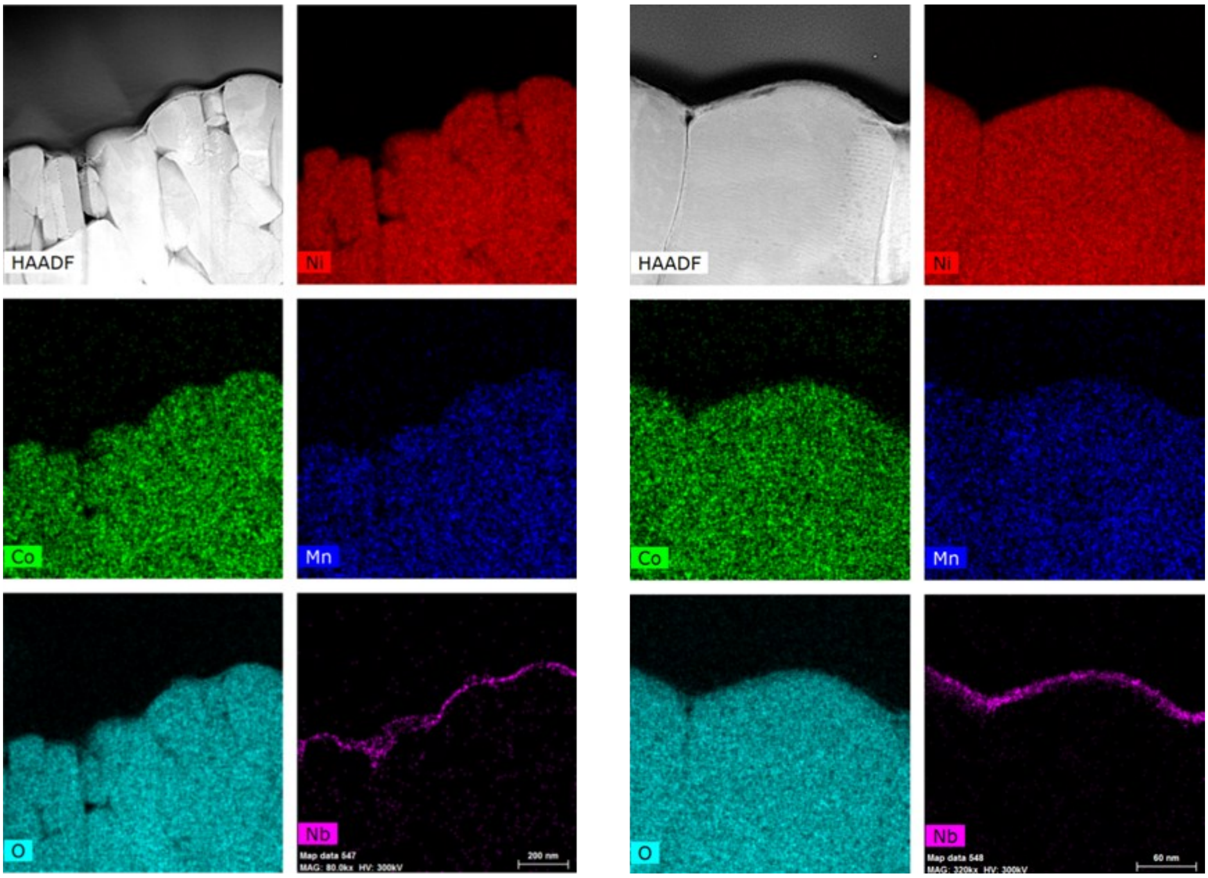

Figure S2. Surface TEM and EDS mapping images of $LiNbO_3$-coated secondary and single particle of NCM electrode.

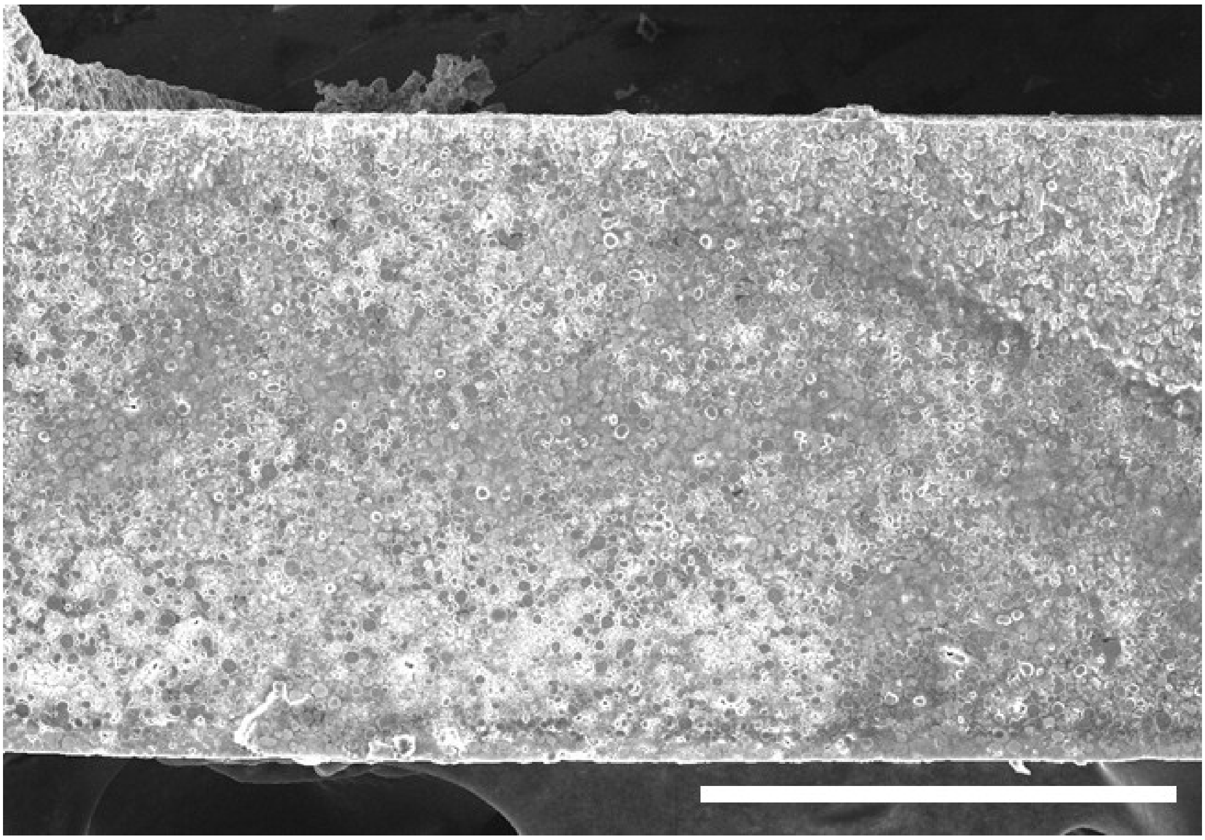

Figure S3. Cross-section SEM images of cathode and electrolyte composite pellet (1:1, v/v).

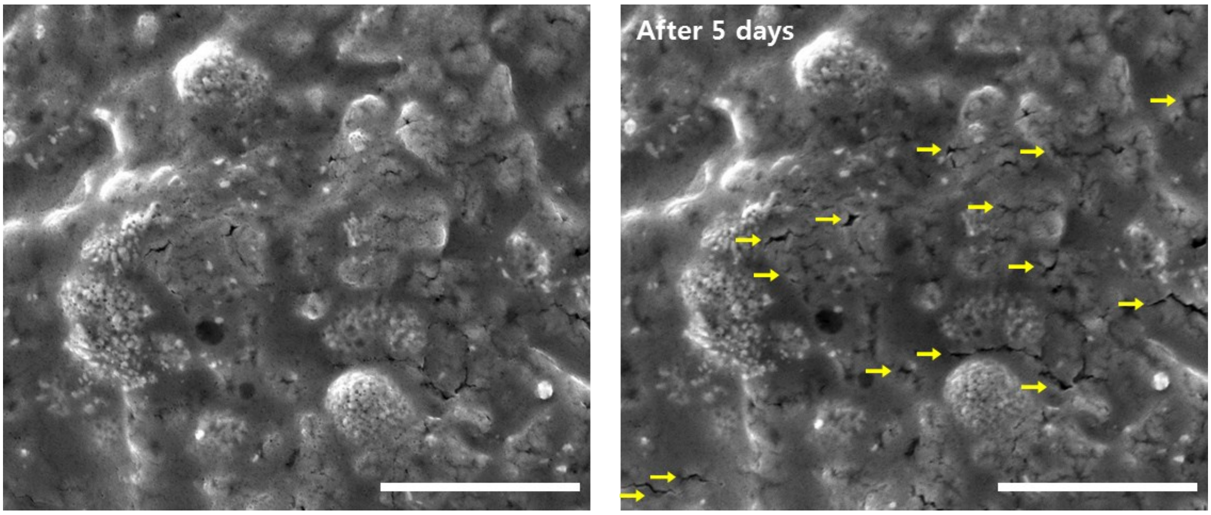

Figure S4. In-situ SEM image during chemical reaction between bare NCM and argyrodite without external pressure in vacuum state. (Left) Fresh composite pellet of bare NCM and argyrodite. (Right) SEM image after 5 days. Yellow arrows indicate microstructural changes. Scale bar is 10 micrometer.

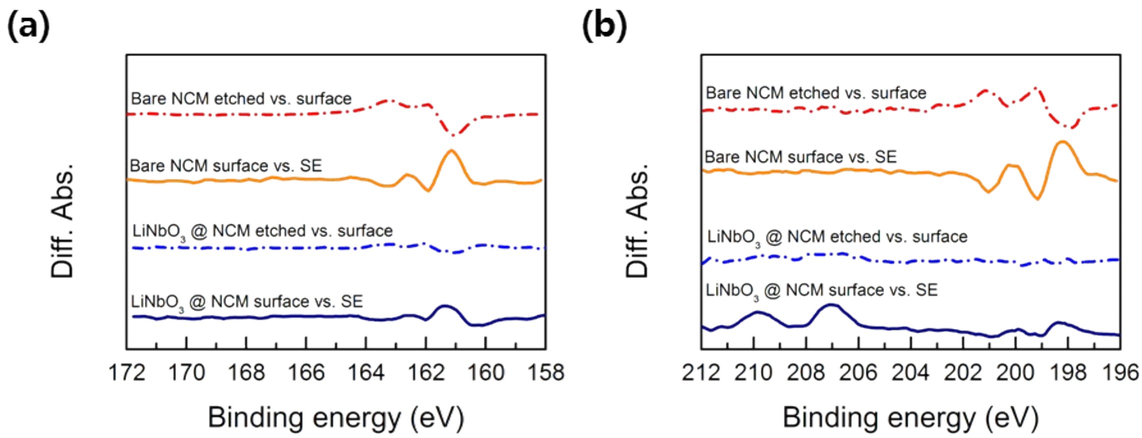

Figure S5. Difference in XPS peak (solid line: surface versus pristine electrolyte; dash-dot line: etched region versus surface) for (a) bare NCM and (b) $LiNbO_3$-coated NCM with argyrodite electrolyte.

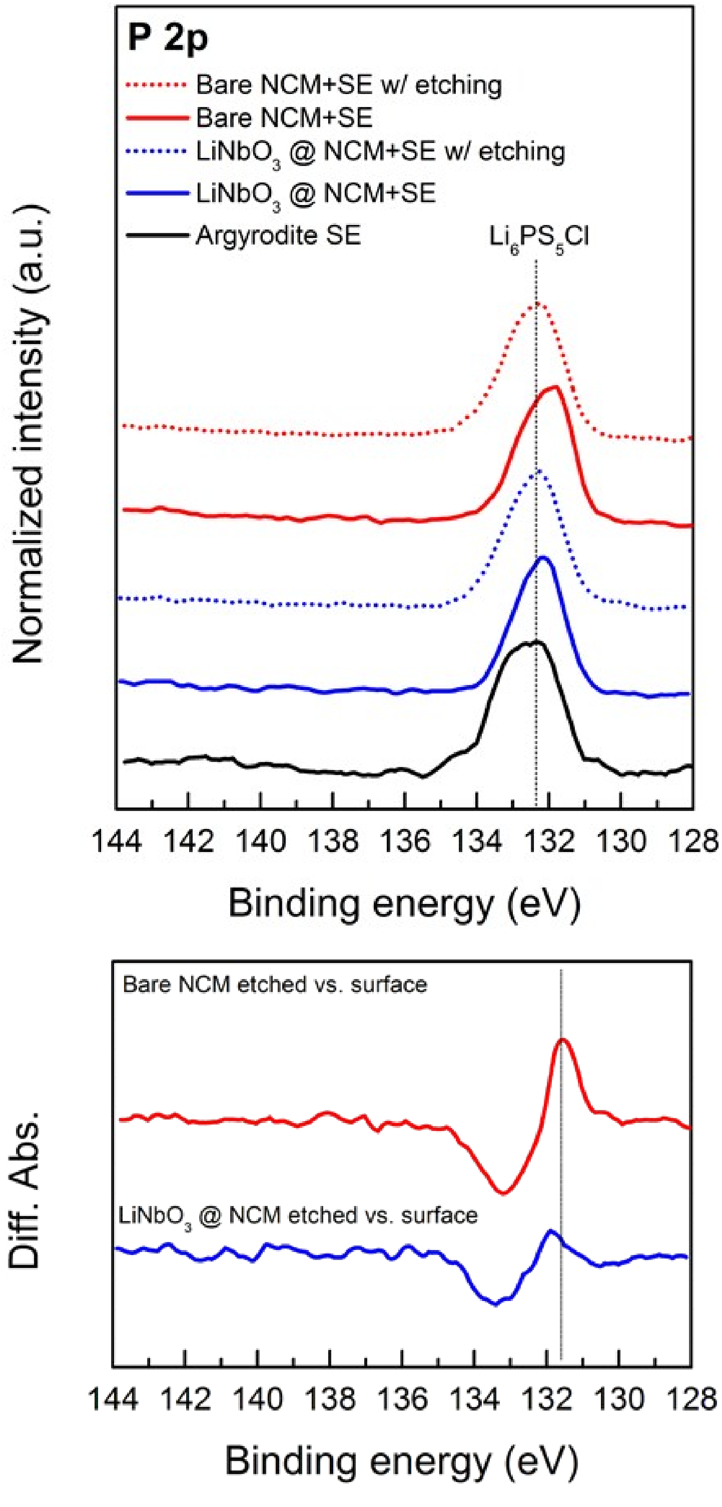

Figure S6. P 2p XPS spectra of aged cell with bare NCM or $LiNbO_3$-coated NCM at the surface (solid line) and after etching (dashed line) compared with that of pristine argyrodite.

Table S1. EIS fitting parameter for bare NCM and argyrodite composite

Bare NCM+SE	Values as a function of time							
	0 h	1.4 h	5.6 h	12.6 h	19.6 h	26.6 h	33.6 h	40.6 h
R_e (Ω)	21.69	27.86	35.78	44.89	51.62	56.62	61.10	64.72
$R_{e,gb}$ (Ω)	50.64	61.35	84.09	122.69	162.59	204.12	244.93	284.47
Q_e (F*cm^{-1}*s$^{\alpha-1}$)	9.24E-7	6.06E-7	4.67E-7	3.70E-7	3.22E-7	2.98E-7	2.80E-7	2.68E-7
α_e	0.520	0.542	0.540	0.531	0.521	0.511	0.503	0.496
C_e (F)	1.22E-7	1.07E-7	8.27E-8	6.05E-8	4.79E-8	4.06E-8	3.60E-8	3.25E-8
R_i (Ω)	27.51	34.49	43.46	52.35	58.36	62.51	66.07	68.92
$R_{i,gb}$ (Ω)	273.99	273.53	339.07	415.81	488.02	555.46	613.79	663.25
Q_i (F*cm^{-1}*s$^{\alpha-1}$)	6.21E-7	4.29E-7	3.45E-7	2.96E-7	2.73E-7	2.65E-7	2.59E-7	2.55E-7
α_i	0.515	0.537	0.534	0.525	0.516	0.506	0.498	0.491
C_i (F)	2.45E-7	1.82E-7	1.38E-7	1.06E-7	8.75E-8	7.72E-8	6.88E-8	6.21E-8
Q_{cpe} (F*cm^{-1}*s$^{\alpha-1}$)	0.03965	0.05099	0.03804	0.02984	0.02527	0.0222	0.02006	0.0184
α_{cpe}	0.769	0.682	0.696	0.700	0.700	0.698	0.696	0.694
T (cm)	0.0318	0.0318	0.0318	0.0318	0.0318	0.0318	0.0318	0.0318
L (H*cm^2)	3.73E-6	4.04E-6	4.60E-6	5.27E-6	5.82E-6	6.34E-6	6.84E-6	7.27E-6
A (cm^2)	1.327	1.327	1.327	1.327	1.327	1.327	1.327	1.327

Table S2. EIS fitting parameter for $LiNbO_3$-coated NCM and argyrodite composite

$LiNbO_3$ coated NCM+SE	Values as a function of time							
	0 h	1.4 h	5.6 h	12.6 h	19.6 h	26.6 h	33.6 h	40.6 h
R_e (Ω)	21.29	19.15	20.98	22.72	23.12	23.84	24.42	24.60
$R_{e,gb}$ (Ω)	296.70	304.88	323.03	343.84	360.41	373.29	385.19	395.99
Q_e ($F*cm^{-1}*s^{\alpha-1}$)	1.06E-06	1.29E-06	1.25E-06	1.20E-06	1.20E-06	1.19E-06	1.17E-06	1.17E-06
α_e	0.440	0.419	0.420	0.422	0.421	0.421	0.421	0.420
C_e (F)	1.78E-7	1.80E-7	1.86E-7	1.92E-7	2.01E-7	2.06E-7	2.06E-7	2.10E-7
R_i (Ω)	17.10	20.34	20.55	20.40	20.55	20.26	20.18	20.55
$R_{i,gb}$ (Ω)	219.22	218.66	226.99	233.04	234.09	236.77	239.09	239.92
Q_i ($F*cm^{-1}*s^{\alpha-1}$)	1.32E-06	1.19E-06	1.25E-06	1.31E-06	1.31E-06	1.36E-06	1.37E-06	1.36E-06
α_i	0.424	0.434	0.427	0.420	0.418	0.414	0.412	0.412
C_i (F)	1.37E-7	1.37E-7	1.36E-7	1.32E-7	1.27E-7	1.28E-8	1.25E-7	1.24E-7
Q_{cpe} ($F*cm^{-1}*s^{\alpha-1}$)	0.02937	0.03063	0.03099	0.03160	0.03265	0.03329	0.03384	0.03448
α_{cpe}	0.805	0.796	0.799	0.800	0.796	0.795	0.793	0.790
T (cm)	0.0318	0.0318	0.0318	0.0318	0.0318	0.0318	0.0318	0.0318
L ($H*cm^2$)	6.90E-06	6.77E-06	6.89E-06	6.99E-06	7.06E-06	7.11E-06	7.17E-06	7.16E-06
A (cm^2)	1.327	1.327	1.327	1.327	1.327	1.327	1.327	1.327

References

1. Kato, Y, *et al.* High-power all-solid-state batteries using sulfide superionic conductors. *Nat. Energy* **1**, 16030 (2016).
2. Manthiram, A, Yu, X, Wang, S. Lithium battery chemistries enabled by solid-state electrolytes. *Nat. Rev. Mater.* **2**, 16103 (2017).
3. Zhang, Z, *et al.* New horizons for inorganic solid state ion conductors. *Energy Environ. Sci.* **11**, 1945-1976 (2018).
4. Kamaya, N, *et al.* A lithium superionic conductor. *Nat. Mater.* **10**, 682 (2011).
5. Seino, Y, Ota, T, Takada, K, Hayashi, A, Tatsumisago, M. A sulphide lithium super ion conductor is superior to liquid ion conductors for use in rechargeable batteries. *Energy Environ. Sci.* **7**, 627-631 (2014).
6. Wang, Y, *et al.* Design principles for solid-state lithium superionic conductors. *Nat. Mater.* **14**, 1026 (2015).
7. Bachman, JC, *et al.* Inorganic solid-state electrolytes for lithium batteries: mechanisms and properties governing ion conduction. *Chem. Rev.* **116**, 140-162 (2015).
8. Zhang, W, *et al.* Degradation mechanisms at the $Li_{10}GeP_2S_{12}/LiCoO_2$ cathode interface in an all-solid-state lithium-ion battery. *ACS Appl. Mater. Interfaces* **10**, 22226-22236 (2018).
9. Han, X, *et al.* Negating interfacial impedance in garnet-based solid-state Li metal batteries. *Nat. Mater.* **16**, 572 (2017).
10. Zhu, Y, He, X, Mo, Y. Origin of outstanding stability in the lithium solid electrolyte materials: insights from thermodynamic analyses based on first-principles calculations. *ACS Appl. Mater. Interfaces* **7**, 23685-23693 (2015).
11. Wenzel, S, *et al.* Direct observation of the interfacial instability of the fast ionic conductor $Li_{10}GeP_2S_{12}$ at the lithium metal anode. *Chem. Mater.* **28**, 2400-2407 (2016).
12. Koerver, R, *et al.* Capacity fade in solid-state batteries: interphase formation and chemomechanical processes in nickel-rich layered oxide cathodes and lithium thiophosphate solid electrolytes. *Chem. Mater.* **29**, 5574-5582 (2017).
13. Walther, F, *et al.* Visualization of the Interfacial Decomposition of Composite Cathodes in Argyrodite-Based All-Solid-State Batteries Using Time-of-Flight Secondary-Ion Mass Spectrometry. *Chem. Mater.* **31**, 3745-3755 (2019).
14. Auvergniot, J, Cassel, A, Ledeuil, J-B, Viallet, V, Seznec, V, Dedryvère, Rm. Interface stability of argyrodite Li_6PS_5Cl toward $LiCoO_2$, $LiNi_{1/3}Co_{1/3}Mn_{1/3}O_2$, and $LiMn_2O_4$ in bulk all-solid-state batteries. *Chem. Mater.* **29**, 3883-3890 (2017).
15. Xiao, Y, Miara, LJ, Wang, Y, Ceder, G. Computational Screening of Cathode Coatings for Solid-State Batteries. *Joule*, (2019).
16. Deiseroth, HJ, *et al.* Li_6PS_5X: a class of crystalline Li-rich solids with an unusually high Li^+ mobility. *Angew. Chem. Int. Ed.* **47**, 755-758 (2008).
17. Rao, RP, Adams, S. Studies of lithium argyrodite solid electrolytes for all-solid-state batteries. *Phys. Status Solidi A* **208**, 1804-1807 (2011).
18. Ohta, N, *et al.* $LiNbO_3$-coated $LiCoO_2$ as cathode material for all solid-state lithium secondary batteries. *Electrochem. Commun.* **9**, 1486-1490 (2007).
19. Asano, T, Yubuchi, S, Sakuda, A, Hayashi, A, Tatsumisago, M. Electronic and ionic conductivities of $LiNi_{1/3}Mn_{1/3}Co_{1/3}O_2$-$Li_3PS_4$ positive composite electrodes for all-solid-state lithium batteries. *J. Electrochem. Soc.* **164**, A3960-A3963 (2017).
20. Yoon, K, Kim, J-J, Seong, WM, Lee, MH, Kang, K. Investigation on the interface between $Li_{10}GeP_2S_{12}$ electrolyte and carbon conductive agents in all-solid-state lithium battery. *Sci. Rep.* **8**, (2018).

21. Jung, SH*, et al.* Li_3BO_3–Li_2CO_3: Rationally designed buffering phase for sulfide all-solid-state Li-ion batteries. *Chem. Mater.* **30**, 8190-8200 (2018).
22. Siroma, Z, Sato, T, Takeuchi, T, Nagai, R, Ota, A, Ioroi, T. AC impedance analysis of ionic and electronic conductivities in electrode mixture layers for an all-solid-state lithium-ion battery. *J. Power Sources* **316**, 215-223 (2016).
23. Siroma, Z, Fujiwara, N, Yamazaki, S-i, Asahi, M, Nagai, T, Ioroi, T. Mathematical solutions of comprehensive variations of a transmission-line model of the theoretical impedance of porous electrodes. *Electrochim. Acta* **160**, 313-322 (2015).
24. Jamnik, J, Maier, J. Treatment of the impedance of mixed conductors equivalent circuit model and explicit approximate solutions. *J. Electrochem. Soc.* **146**, 4183-4188 (1999).
25. Kaiser, N, Spannenberger, S, Schmitt, M, Cronau, M, Kato, Y, Roling, B. Ion transport limitations in all-solid-state lithium battery electrodes containing a sulfide-based electrolyte. *J. Power Sources* **396**, 175-181 (2018).
26. Wenzel, S, Sedlmaier, SJ, Dietrich, C, Zeier, WG, Janek, J. Interfacial reactivity and interphase growth of argyrodite solid electrolytes at lithium metal electrodes. *Solid State Ionics* **318**, 102-112 (2018).
27. Benaissa, K, Ashrit, P, Bader, G, Girouard, FE, Truong, V-V. Electrical and optical properties of $LiNbO_3$. *Thin Solid Films* **214**, 219-222 (1992).
28. Irvine, JT, Sinclair, DC, West, AR. Electroceramics: characterization by impedance spectroscopy. *Advanced Materials* **2**, 132-138 (1990).
29. Koerver, R*, et al.* Chemo-mechanical expansion of lithium electrode materials–on the route to mechanically optimized all-solid-state batteries. *Energy Environ. Sci.* **11**, 2142-2158 (2018).
30. Luo, P*, et al.* Targeted Synthesis of Unique Nickel Sulfide (NiS, NiS2) Microarchitectures and the Applications for the Enhanced Water Splitting System. *ACS Appl. Mater. Interfaces* **9**, 2500-2508 (2017).
31. Karthikeyan, R, Thangaraju, D, Prakash, N, Hayakawa, Y. Single-step synthesis and catalytic activity of structure-controlled nickel sulfide nanoparticles. *CrystEngComm* **17**, 5431-5439 (2015).
32. Lin, L, Liang, F, Zhang, K, Mao, H, Yang, J, Qian, Y. Lithium phosphide/lithium chloride coating on lithium for advanced lithium metal anode. *Journal of Materials Chemistry A* **6**, 15859-15867 (2018).
33. Auvergniot, J, Cassel, A, Foix, D, Viallet, V, Seznec, V, Dedryvère, R. Redox activity of argyrodite Li_6PS_5Cl electrolyte in all-solid-state Li-ion battery: An XPS study. *Solid State Ionics* **300**, 78-85 (2017).